Sensors and Actuators B 240 (2017) 586–594

Contents lists available at ScienceDirect

Sensors and Actuators B: Chemical

journal homepage: www.elsevier.com/locate/snb

Near–infrared electrochemiluminesence biosensor for high sensitive detection of porcine reproductive and respiratory syndrome virus based on cyclodextrin-grafted porous Au/PtAu nanotube

Kang Shao [1], Chenjun Zhang [1], Shiyi Ye, Kai Cai, Long Wu, Biru Wang, Chenchen Zou, Zhicheng Lu, Heyou Han *

State Key Laboratory of Agricultural Microbiology, College of Science, College of Food Science and Technology, Huazhong Agricultural University, Wuhan, 430070, PR China

ARTICLE INFO

Article history:
Received 28 April 2016
Received in revised form 14 August 2016
Accepted 28 August 2016
Available online 29 August 2016

Keywords:
Porcine reproductive and respiratory syndrome virus
Near–infrared
Electrochemiluminescence
PtAu nanotube
Enzyme catalysis

ABSTRACT

Self-supported one-dimensional nanocatalysts with better electrical transport and less vulnerable to dissolution and aggregation than zero-dimensional nanocrystals have aroused particular attention in mimic-enzyme catalysis. Herein, the porous Au/PtAu bimetallic heterojunction nanotube (PtAu BNT) as a remarkable catalyst was firstly introduced into the near–infrared electrochemiluminesence (NIR ECL) immunoassay for enhancing detection sensitivity of porcine reproductive and respiratory syndrome virus (PRRSV). Meanwhile, the unique and strong host-guest recognition between β-cyclodextrin and adamantine was chose as the linker to assemble the PtAu BNTs catalysts onto PRRSV antibody, which clearly surpassed the unstable electrostatic assembly between cationic surfactant and biosamples. The formed supramolecular "bridge" could extend the space to accommodate more PtAu BNTs catalysts and reduce the blocking effect. The fabricated sandwich immunosensor exhibited excellent analytical performance for PRRSV with a better linear detection range from $1{:}10^3$ to $1{:}10^6$ (dilution ratio) and a sensitive detection limit (10.8 pg/mL). Good stability, acceptable reproducibility and accuracy of the immunosensor suggested its potential applications in clinical diagnostics.

© 2016 Elsevier B.V. All rights reserved.

1. Introduction

Porcine reproductive and respiratory syndrome virus (PRRSV) is a small, enveloped positive single-stranded RNA virus that causes reproductive failure in breeding swine and respiratory problems in young pigs [1]. PRRSV has become a significant pathogen of swine herds worldwide, with new disease phenotypes emerging constantly, leading to severe economic losses in global animal husbandry [2]. Accurate detection of disease marker at low concentrations is crucially important for successful infectious disease control, which can facilitate early-stage disease detection. Recently, increasing false-positive detections of PRRSV were reported using reverse-transcription polymerase chain reaction (PCR), which were commonly used in laboratory diagnosis [3]. Therefore, combination of different assays is needed for accurate early-stage disease detection [4]. A better alternative electrogenerated chemiluminescence (ECL) technology has attracted increasing interest in biosensing applications because of its high sensitivity, wide dynamic concentration response range, as well as its potential and spatial controlment [5].

Currently, the ECL emissions from traditional emitters, such as luminol [6], polyaromatic hydrocarbons [7] and $Ru(bpy)_3^{2+}$ [8] are alsways interfered by background signals of biosamples. Development of near–infrared (NIR, emission 650–900 nm) ECL analysis could avoid background signals in visible light range and reduce photochemical damage of biological samples [9]. Great efforts have been made toward the fundamental properties and theoretical explanations of NIR-emitting QDs ECL [10]. However, few studies are focused on NIR QDs-based ECL biosensors [11], because relatively weak ECL signal intensity and unexpected ECL signal interference of persulfate [12]. Thus, it is imperative to explore new signal amplification strategy and restrain signal interference by persulfate itself. The NIR QDs-H_2O_2/O_2 ECL system is an alternative co-reaction system but needs signal amplification [13].

Inspired by our proposed amplification strategy, the NIR ECL can be improved via increasing the amount of signal labels or raising the efficiency of single signal label in single-pass ECL behavior [14]. By means of some "bridge" linkers, such as streptavidin-biotin [15] and cyclodextrin-adamantane [16], more signal labels

* Corresponding author.
E-mail address: hyhan@mail.hzau.edu.cn (H. Han).
[1] Both authors contributed equally to this work.

http://dx.doi.org/10.1016/j.snb.2016.08.162
0925-4005/© 2016 Elsevier B.V. All rights reserved.

could be anchored in an extended space above antibody or DNA, which could not only reduce the blocking effect but also expand space. Beta-cyclodextrin (β-CD), a cyclic oligosaccharide composed of seven glucopyranose units, could form stable "bridge" linker with various guest molecules by the host-guest interaction owing to their special molecular structures-hydrophobic internal cavity and hydrophilic external surface [17]. Recently, Ju's group achieved signal-enhanced electrochemical bioassay relying on host-guest interaction between β-CD functionalized AuPd bimetallic nanoparticles and adamantine (Ada) [18]. By theoretical calculation, approximately seven AuPd labels can be connected with a single antibody. On the other hand, enzyme catalysis plays an important role in raising the efficiency of ECL signal label [19]. Nevertheless, natural enzymes have the restrictions of instability, long-time consumption and high-cost purification processes. Therefore, a variety of nanostructures have been developed as artificial enzymes, mainly including Fe-based nanoparticles [20], graphene oxide based-nanoparticles [21], metallic nanoparticles [22] and alloy nanoparticles [23]. Especially, porous materials exhibit much higher catalytic activity than do their bulk counterparts. As known to us all, one-dimensional nanocrystals, such as nanowires and nanotubes, have better electrical transport and are less vulnerable to dissolution and aggregation than zero-dimensional nanocrystals when used as self-supported catalysts [24]. Nonetheless, little is known about porous nanotubes and even heterojunction nanotubes as artificial enzymes. Recently, we have synthesized quasi-one-dimensional Au/PtAu heterojunction nanotubes by the heterogeneous nucleation and growth of Au on Te/Pt core-shell nanostructures in aqueous solution [25]. Thus, introducing porous one-dimensional heterojunction nanotube with high catalytic activity into NIR-ECL bioassay would effectively reduce the amount of catalyst and greatly increase the detection sensitivity of bio-samples, which to our knowledge, has never been reported before.

However, the Au/PtAu heterojunction nanotube compactly coated by the long chain cationic surfactant cetyltrimethyl ammonium bromide (CTAB) is different to connect biosamples tightly, which greatly restrict its biological application. Herein, we utilized host-guest recognition to prepare a CTAB-free porous Au/PtAu heterojunction nanotube-cyclodextrin composite and integrated the NIR ECL of the core-shell CdTe/CdS QDs-H_2O_2 system to prepare a synergistically amplified NIR ECL immunosensor for ultrasensitive detection of PRRSV. The porous PtAu BNT instead of the traditional enzyme was used as mimic-enzyme catalyst to improve the efficiency of single signal label. The ECL intensities increased regularly with the increase of PtAu BNTs, which provide the basis of quantitative analysis. On the other hand, more PtAu BNTs could attach firmly to the single antibody leading to "bridge" amplification based on the supramolecular recognition between β-CD and Ada. The sandwich immunosensor can be fabricated using the specific binding of the antibody (Ab_1) to PRRSV and the labeled secondary antibody (Ab_2). The novel ECL biosensor was successfully applied to the detection of PRRSV and presented an excellent performance.

2. Experimental

The used agents and instruments and the detailed preparation processes of Au NPs, NIR-emitting CdTe/CdS $core_{small}/shell_{thick}$ QDs and Te nanowires are described in Supporting information.

2.1. Preparation of porous PtAu BNTs-CD composite

The porous PtAu bimetallic nanotubes were synthesized as reported in our latest work with minor modifications [25]. Briefly, Te nanowires (ca. 0.04 mM) were dispersed in an aqueous solution of CTAB (5 mM, 50 mL) with constant magnetic stirring at 30 °C. An aqueous solution of NaOH (0.1 M, 0.2 mL) and K_2PtCl_6 (ca. 0.01 mM) was added into the solution of CTAB, which changed from blue to grey-black after 30 min, indicating the formation of Te/Pt core-0shell nanostructures. Then, a certain amount of $HAuCl_4$ was added to the solution of CTAB and the solution turned gray-black after 25 min, thus indicating the formation of PtAu bimetallic nanotubes (PtAu BNTs). The mixture was subjected to a centrifugation/wash cycle to remove most of the matrices.

Scheme 1B showed the proposed formation process of porous PtAu bimetallic nanotube-cyclodextrin composite (PtAu BNTs-CD). Firstly, 1 mL of porous PtAu BNTs were subjected to three centrifugation/wash cycles at 12,000 rpm for 15 min and resuspended in 5 mM CTAB solution. Next, 1.5 mL of 5 mM SH-β-CD was added dropwise into the dispersion under stirring. After the mixture was gently shaken overnight at room temperature, the formed PtAu BNTs-CD composite was collected by two times of centrifugation at 12,000 rpm for 15 min with 5 mM CTAB as the washing solution. Finally, the composite was redispersed in 2 mL of 5 mM CTAB solution and stored at 4 °C for further use.

2.2. Preparation of Ada-***Ab conjugates***

Adamantanecarboxylic acid (33 mg) was suspended in 40 mL of water followed by adding 20 μL of 1 M NaOH to obtain a clear solution, which was immediately diluted to 100 mL. EDC (10 mg) and NHS (10 mg) were added to 2 mL of Ada solution and then mixed with 2 mL of PBS (50 mM, pH 7.4). After the mixture was gently shaken at room temperature for 30 min, PRRSV antibody solution (20 μg/mL, 1 mL) was injected into this mixture and incubated overnight at 4 °C. Subsequently, the obtained mixture was dialyzed against PBS (50 mM, pH 7.4) to remove the excess Ada. Finally, the Ada-Ab conjugates were gathered and stored at 4 °C for further use.

2.3. Preparation of porous PtAu BNTs-***CD@Ada-Ab conjugates***

The porous PtAu BNTs-CD composite and Ada-Ab conjugates were mixed at an approximate molar ratio of 1:10 overnight at room temperature. Then, the conjugates were collected by two times of centrifugation at 12,000 rpm for 15 min and then redispersed in 5 mM CTAB solution containing 1% BSA and stored at 4 °C for further use.

2.4. Fabrication of the sandwich immunosensor

Scheme 1A represented the preparation of the biosensor. The polished and subsequently washed glassy carbon electrode (GCE, diameter of 3 mm) was dried with high-purity nitrogen gas for the next modification process. Five microliters of carbon nanotubes (CNTs) solution, 6 μL of CdTe/CdS $core_{small}/shell_{thick}$ QDs solution and 6 μL of chitosan solution (0.025%) were pipetted one after another onto the center of the pretreated GCE and dried at room temperature for over 3 h. Then, CH/QDs/CNTs/GCE was incubated in 100 μL of Au NPs solution for 2 h, followed by rinsing twice with PBST. After that, 10 μL of PRRSV Ab_1 was pipetted onto the Au/CH/QDs/CNTs/GCE surface and then covered with a pipette tip for 12 h at 4 °C. Next, the modified electrode was rinsed with PBST to remove physically absorbed antibody and then incubated in 100 μL 1% BSA solution for 1 h at 37 °C to block possible remaining active sites and avoid the nonspecific adsorption. After washing thoroughly with PBST, the Ab_1/Au/CH/QDs/CNTs/GCE was incubated in 60 μL of PRRSV suspension for 1 h at 37 °C and then washed with PBST. Finally, the Ag/Ab_1/BSA/Au/CH/QDs/CNTs/GCE was incubated in 100 μL of PtAu BNTs-CD@Ada-Ab conjugates for 1 h at 37 °C,

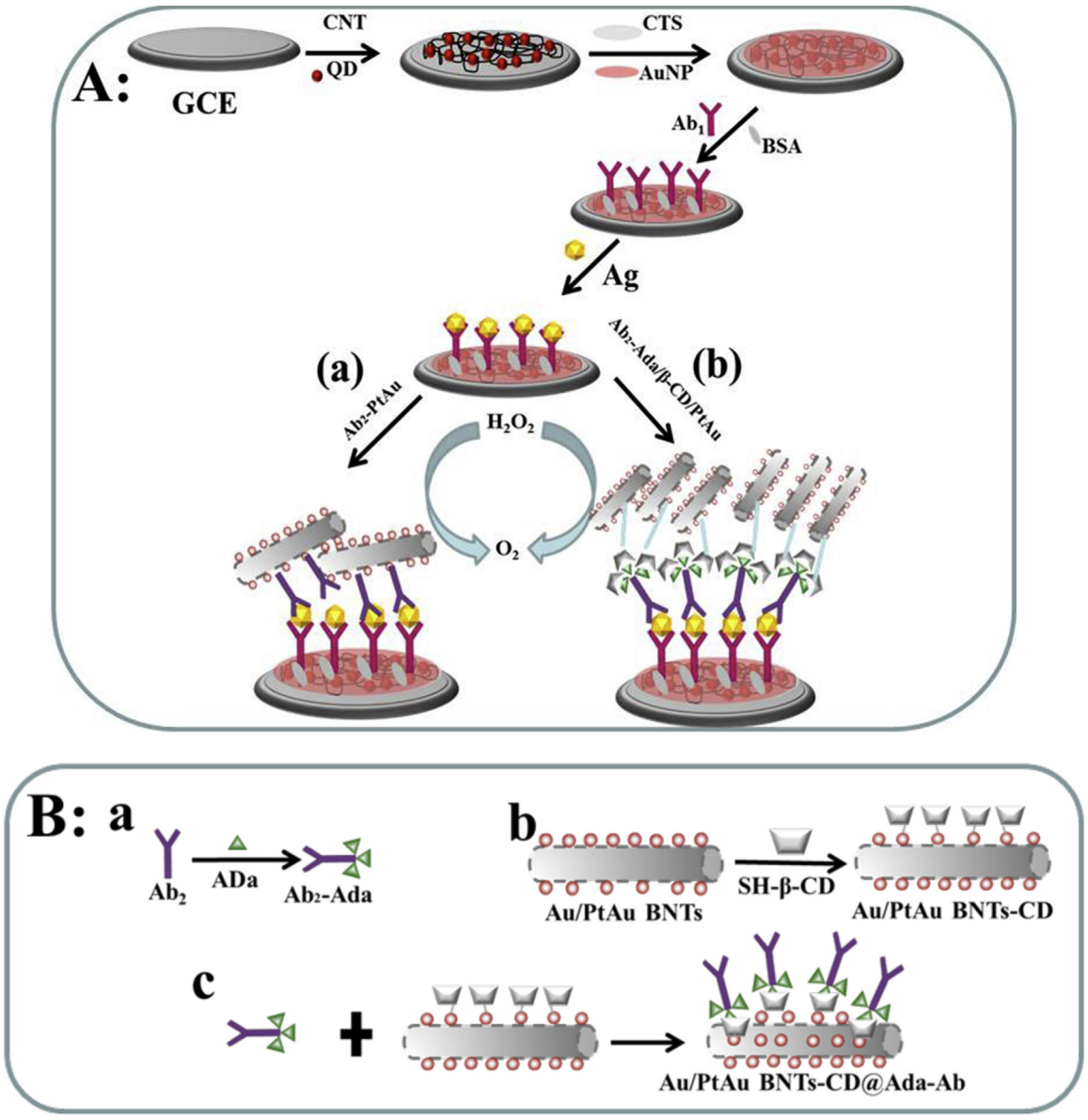

Scheme 1. (A) Schematic illustration of ECL biosensors for detection of PRRSV (a) without Ada and β-CD (b) with Ada and β-CD. (B) The fabrication procedures of (a) Ab_2-Ada (b) PtAu BNTs-CD (c) PtAu BNTs-CD@Ada-Ab_2.

and then washed thoroughly with PBST to remove nonspecifically bound conjugates for the subsequent ECL characterization assays.

3. Results and discussion

3.1. Characterization of the nanomaterials

Transmission electron microscopy (TEM) was initially used to observe the microstructure of the Te nanowires, PtAu BNTs, CNTs, Au NPs and CdTe/CdS QDs. As shown in Fig. 1A, Te nanowire (Te NWs) presented a uniform rhabdoid structure with a mean diameter of 20 nm and a length of 500 nm. In Fig. 1B, the hollowed-out and porous Pt/Au bimetallic nanotube synthesized from Te NWs templates were interspersed with spherical Pt/Au nanoparticles with no individual nanoparticles observed in the surroundings, indicating that nanoparticles heterogeneously nucleate and grow directly on the surface of the framework. To further verify the Pt/Au element distribution in the bimetallic nanotube, the nanotube was characterized by high-angle annular dark-field (HAADF) scanning transmission electron microscopy (STEM). Fig. 1D respectively showed the HAADF-STEM images of the bimetallic nanotube and the selected-area in the HAADF-STEM image of bimetallic nanotube. The Pt and Au elemental mappings of the selected-area in the bimetallic nanotube showed in Fig. 1E and F indicated that elemental Au and Pt were distributed on every component of the heterojunction nanotube. Fig. S1A showed CNTs possessed the spindly and interlaced tubular structures. Spherical Au NPs with a uniform size (~25 nm, Fig. S1B) showed a strong characteristic absorption peak at 523 nm due to surface plasmon resonance (Fig. S1D). Under ultraviolet light irradiation, the MPA-CdTe/CdS coresmall/shell thick QD with 3.5 nm size (Fig. S1C) and 7.53 nm average hydrodynamic size (Fig. S1E) showed a −25.2 mV zeta-potential (Fig. S1F). As displayed in Fig. 2A, a clear characteristic absorption peak at 650 nm and a sharp fluorescent emission peak at 710 nm were observed, revealing that the CdTe/CdS coresmall/shell thick QD is NIR QD.

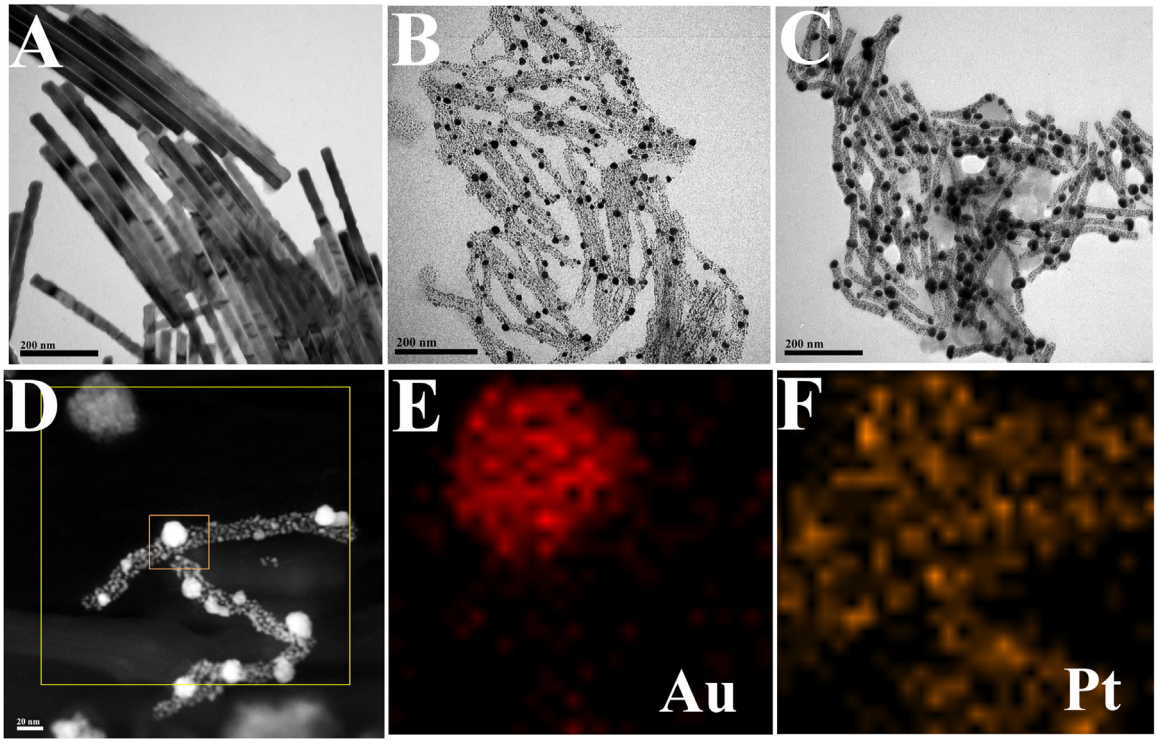

Fig. 1. TEM images of (A) Te NWs, (B) porous PtAu BNTs and (C) PtAu BNTs-CD@Ada-Ab_2. (D, E) HAADF-STEM images and (F) HAADF-STEM energy-dispersive X-ray spectroscopy (EDX) mapping image of PtAu BNTs-CD.

3.2. Characterization of the porous PtAu BNTs-***CD@Ada-Ab$_2$*** ***conjugates***

Firstly, the successful preparation of PtAu BNTs-CD@Ada-Ab_2 conjugates can be directly observed in Fig. 1C. Compared to the equally distributed individual PtAu BNT in Fig. 1B, obvious aggregation and conglutination were observed among most PtAu BNTs in Fig. 1C, indicating the successful formation of PtAu BNTs-CD@Ada-Ab_2 conjugates, which can also be verified by the ultraviolet absorption spectrum. As shown in Fig. 2B, the characteristic absorption peaks of PtAu BNTs emerged at ~260 nm and ~530 nm (curve a). With PtAu BNTs combined to SH-β-CD (curve b), a red shift occurred, which was attributed to the presence of SH-β-CD, indicating the successful fabrication of PtAu BNTs-CD conjugates. After the host-guest recognition between PtAu BNTs-CD and Ada-Ab, two characteristic absorption peaks emerged at about 280 nm and 530 nm, which respectively corresponding to the characteristic absorption peaks of PRRSV Ab and PtAu BNTs, which further confirmed the successful formation of PtAu BNTs-CD@Ada-Ab_2 conjugates. The combination of PtAu BNTs-Ab by electrostatic adsorption can be confirmed in the same way shown in Fig. 2B (curve d) and Fig. 2C.

Additionally, X-ray photoelectron spectroscopy curves of Au4f, Pt4f, N1s and S2p were recorded to further identify the formation of PtAu BNTs-CD@Ada-Ab_2 conjugates (Fig. 2D, E and F). The binding energies of Pt4f and Au4f from PtAu BNTs were 71.94 eV and 83.7 eV, which were lower than that of PtAu BNTs-CD@Ada-Ab_2 (73.14 eV and 91.03 eV) (Fig. 2E). In Fig. 2F, the new S2p binding energy could be ascribed to the sulfur from the disulfide bond in protein (168.47 eV). In addition, conjugation with Ada-Ab_2 on PtAu BNTs-CD resulted in an increase in the relative elemental compositions of oxygen, nitrogen, and sulfur and a decrease in the irrelative elemental compositions of platinum and gold (Fig. 2D and Table S1). All these facts confirmed that PtAu BNTs-CD@Ada-Ab_2 conjugates were successfully fabricated.

3.3. ECL of CdTe/CdS $core_{small}$/$shell_{thick}$ QDs-H_2O_2 system

The ECL performance of NIR QDs was closely related to the triggering potential, scan rates and pH of PB solution, thus a series of optimization experiments were carried out concerning these variables. As shown in Fig. 3A, the ECL intensity showed an increase with the decrease of triggering potential first, followed by a gradual decrease after reaching the peak value. The optimal scan potential window was 0 ~ −1.5 V. Similarly, the optimal scan rate was 0.3 V/s (Fig. 3B). In Fig. 3C, the ECL signal increased obviously with increasing pH, and reached a plateau after pH 8.0. Considering the physiological pH and ECL response of QDs, pH 7.4 was defined as the optimal pH of PB solution.

To explore the role of oxygen in the QDs−H_2O_2 ECL system, three different PB testing solutions were pretreated with air, nitrogen and oxygen for 15 min, respectively. As displayed in Fig. 3D, almost no ECL signal were detected if there is no oxygen in PB testing solution (curve e). With increasing dissolved oxygen concentration, the ECL intensity enhanced greatly (curve d and f), indicating that oxygen plays a vital role in QDs−H_2O_2 ECL system, which also verified the feasibility of improving ECL on the basis of enzyme catalysis.

As shown in Fig. 3E, a significant ECL peak of NIR QDs was observed around −1.5 V. The inset indicated the cyclic voltammetry (CV) of NIR QDs-H_2O_2 at the base condition, which was related to a possible reaction mechanism for the ECL of NIR QDs. Based on the aforementioned results and some previous studies [26], a possible reaction mechanism is proposed as follows:

$$\text{NIR QDs} + e \rightarrow \text{NIR QDs}^- \quad (1)$$

$$O_2 + H_2O + 2e \rightarrow OOH^- + OH^- \text{or} \quad (2)$$

$$H_2O_2 + OH^- \rightarrow OOH^- + H_2O \quad (3)$$

$$\text{NIRQDs}^- + OOH^- + H_2O \rightarrow 3OH^- + 2\,\text{NIR QDs}^* \quad (4)$$

$$\text{NIR QDs}^* \rightarrow \text{NIR QDs} + h\upsilon \quad (5)$$

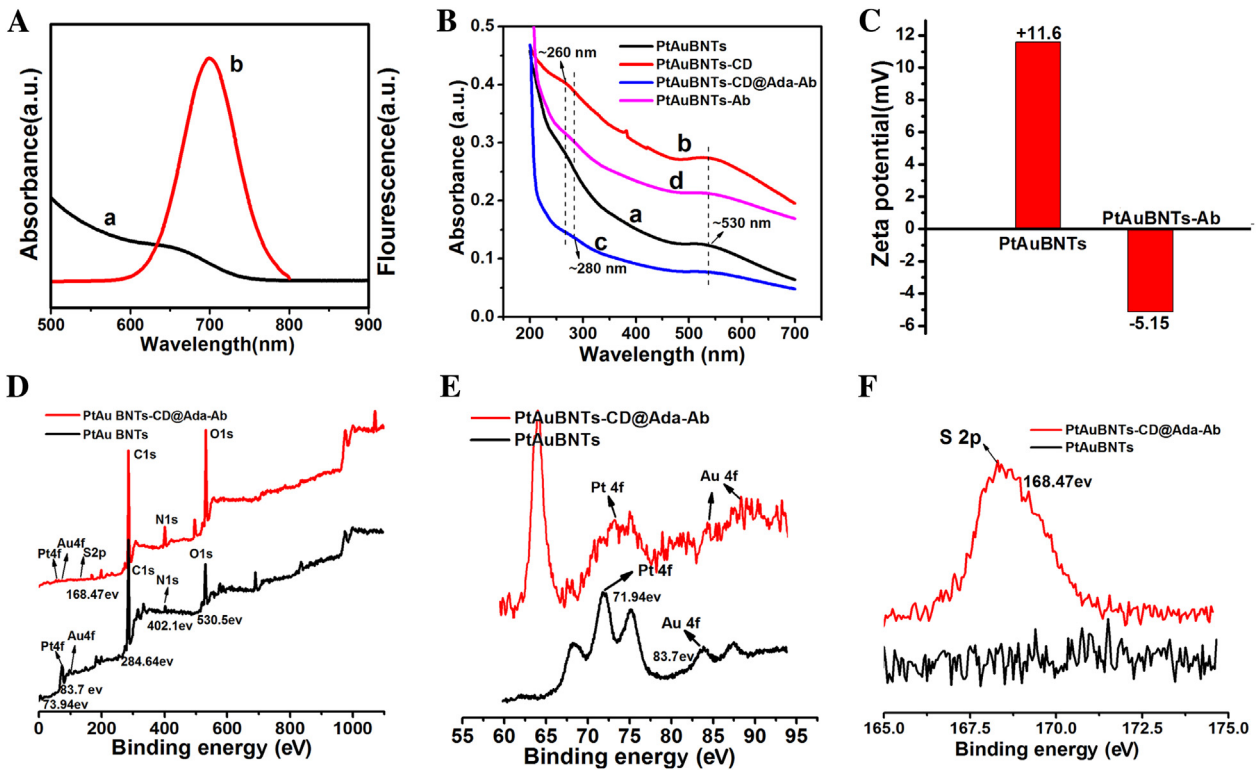

Fig. 2. UV–vis absorption spectra of (A) NIR-QDs and (B) PtAu BNTs (curve a); PtAu BNTs-CD (curve b); PtAu BNTs-CD@Ada-Ab (curve c) and PtAu BNTs-Ab (curve d). (C) Zeta potential of PtAu BNTs-Ab. (D, E and F) XPS analysis of PtAu BNTs and PtAu BNTs-CD@Ada-Ab.

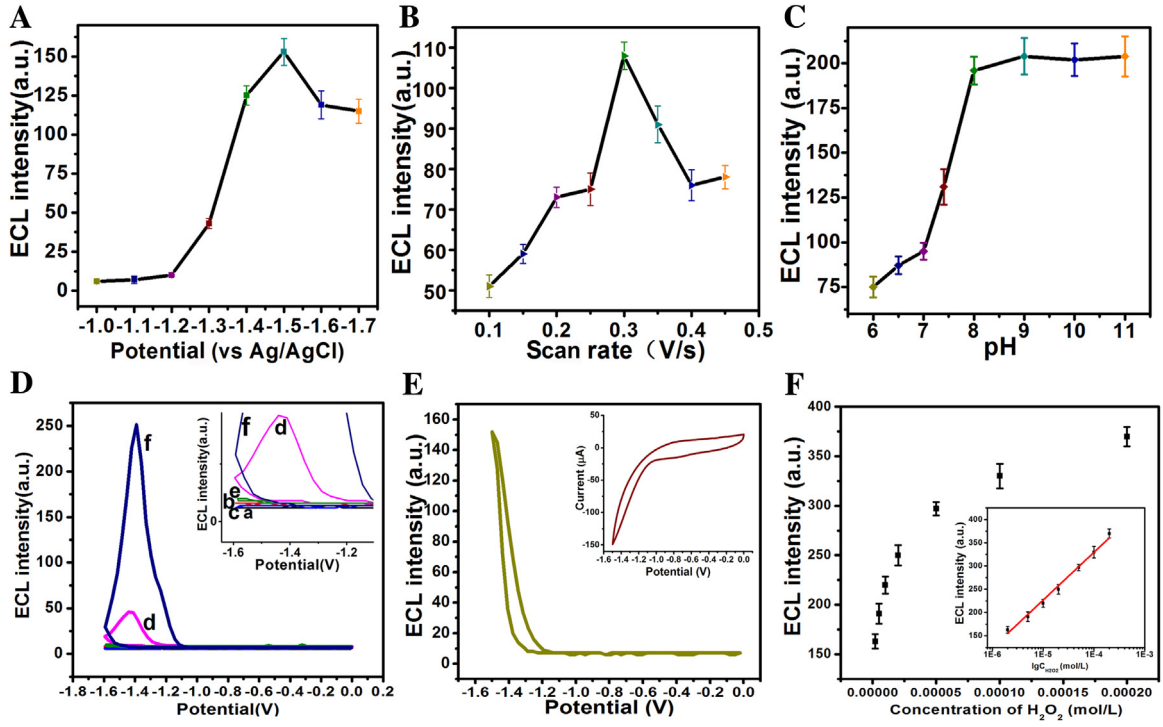

Fig. 3. ECL responses to (A) triggering potential, (B) scan rate and (C) pH. (D) The relation between ECL of QDs and H_2O_2/O_2. (E) ECL-potential curves of QDs-H_2O_2 under optimum conditions. The inset was CV of QDs-H_2O_2. (F) Calibration curve for H_2O_2 determination.

Most ECL emissions are often generated via a so-called pre-annihilation and co-reaction mechanisms. In our study, the dissolved oxygen was reduced and the reduced product OOH^- was one of the co-reactants which participated in the ECL reaction when the electrode potential was scanned from 0 to −1.5 V. At the basic condition, H_2O_2 was liable to produce OOH^-, which could react with NIR QDs$^-$ to generate more NIR QDs*, leading to a higher ECL intensity.

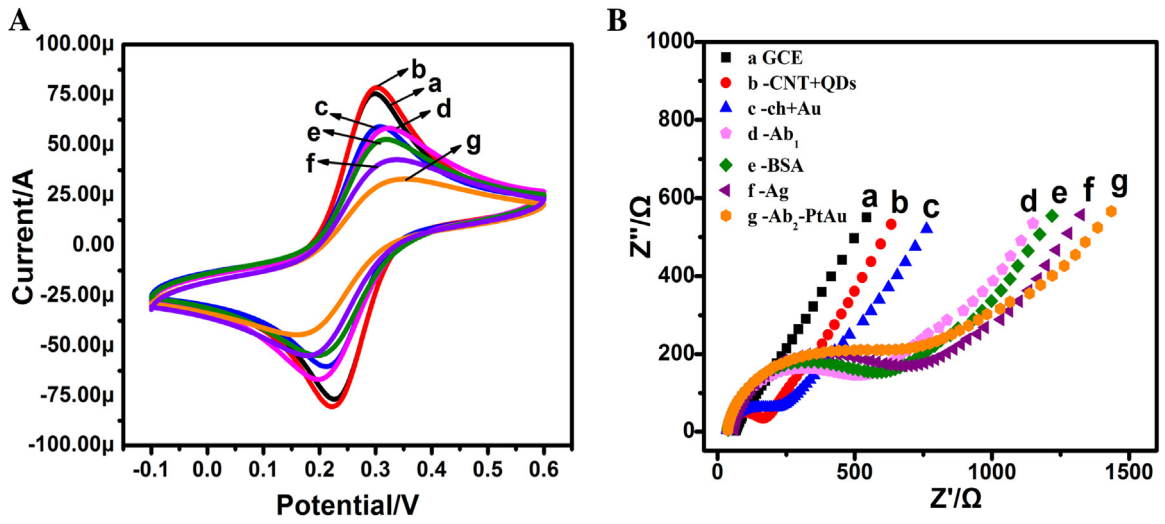

Fig. 4. CV (A) and EIS (B) of (a) bare GCE, (b) CNTs/GCE, (c) Au/CH/QDs/CNTs/GCE, (d) Ab_1/Au/CH/QDs/CNTs/GCE, (e) BSA/Ab_1/Au/CH/QDs/CNTs/GCE, (f) Ag/BSA/Ab_1/Au/CH/QDs/CNTs/GCE, (g) PtAu BNTs-CD@Ada-Ab_2/Ag/BSA/Ab_1/Au/CH/QDs/CNTs/GCE.

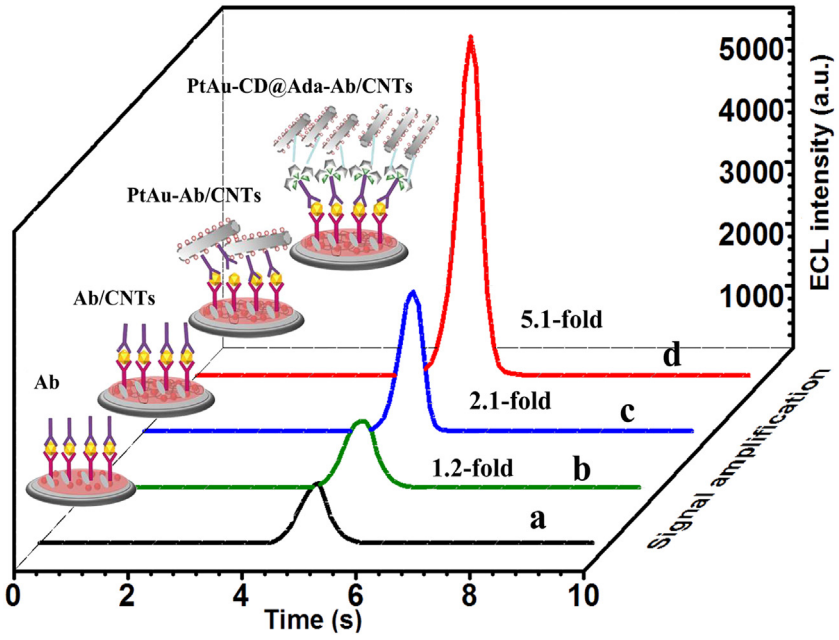

Fig. 5. ECL responses of (a) Ab_2/PRRSV/BSA/Ab_1/Au/CH/QDs/GCE, (b) Ab_2/PRRSV/BSA/Ab_1/Au/CH/QDs/CNTs/GCE, (c) PtAu BNTs/Ab_2/PRRSV/BSA/Ab_1/Au/CH/QDs/CNTs/GCE and (d) PtAu BNTs-CD@Ada-Ab_2/PRRSV/BSA/Ab_1/Au/CH/QDs/CNTs/GCE.

The relationship between ECL intensity of NIR QDs and the concentration of H_2O_2 was showed in Fig. 3F. The ECL intensity was linearly increased with increasing concentration of H_2O_2. The linear regression equation obtained from the calibration curve (the inset) was $y = 102.65x + 740.06$ ($R^2 = 0.9904$) and the linear range was $2.0 \times 10^{-4} \sim 2.0 \times 10^{-6}$ mol/L.

3.4. Characterization of the ECL immunosensor

Cyclic voltammetry (CV) and electrochemical impedance spectroscopy (EIS) were used to verify the assembly process of the modified electrodes step by step. Fig. 2A showed the CV curves characterizing the fabrication procedures of the modified GCE using $[Fe(CN)_6]^{4-}/[Fe(CN)_6]^{3-}$ as electroactive probes. The bare GCE exhibited a couple of reversible redox peaks (curve a). After modified with CNTs, the peak currents of the electrode increased mildly. However, the potential difference (△E) increased slightly between the oxidation peak and reduction peak because of the hydrophobicity of CNTs and the charge repulsion between CNTs and $[Fe(CN)_6]^{4-}/[Fe(CN)_6]^{3-}$ electroactive probes (curve b). The better performance of the modified electrode was attributed to the good electrical conductivity of CNTs. Obvious decrease was observed in the amperometric signal (curve c) when QDs, CH and AuNPs were immobilized on CNTs/GCE. With a further decrease in the peak currents in the CV, the gap between the anodic and cathodic peaks became wider in subsequent stepwise construction process of Ab_1, BSA, PRRSV and PtAu BNTs-CD@Ada-Ab_2. This phenomenon was ascribed to the electron inert properties, blocking the electron transfer and mass transfer of $[Fe(CN)_6]^{4-}/[Fe(CN)_6]^{3-}$ ions at the Au/CH/QDs/CNTs/GCE surface. These results demonstrated the successful fabrication of the ECL biosensor for detection of PRRSV.

Additionally, EIS was also used to monitor the changes of surface features in modified electrodes in the assembly process (Fig. 4B). The diameter of the semicircle in a higher frequency range of the

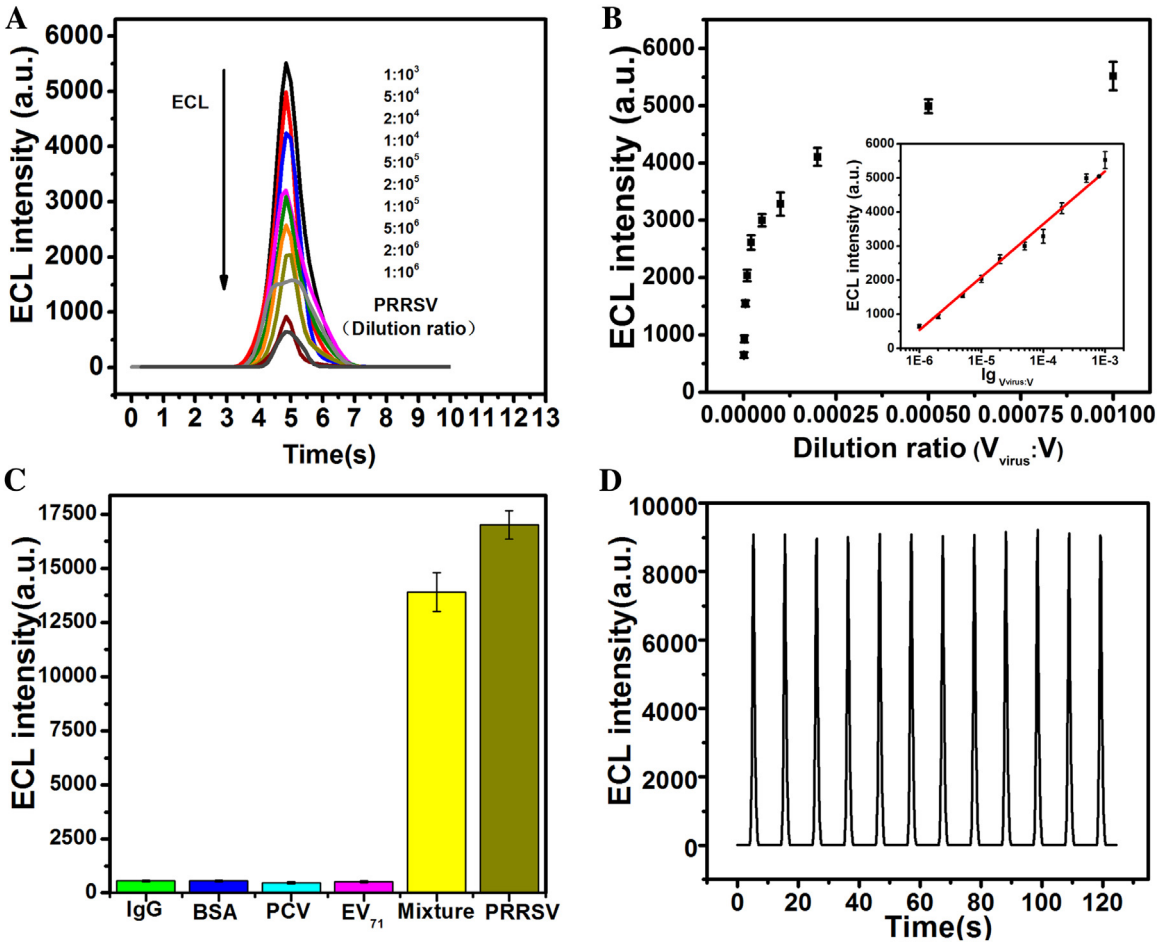

Fig. 6. (A) ECL profiles of the biosensor at different dilution ratios of PRRSV (a–j) $1{:}10^3$–$1{:}10^6$ in 0.1 M pH 7.4 PB solution containing 0.01 M H_2O_2 and in the potential range from 0 V to −1.5 V at a scan rate of 300 mVs^{-1}. (B) Calibration curve for determination of PRRSV. (C) Specificity of IgG, BSA, PCV, EV_{71}, mixed sample and PRRSV. (D) ECL emission from PtAu BNTs-CD@Ada-Ab_2/PRRSV/BSA/Ab_1/Au/CH/QDs/CNTs/GCE under continuous CVs for 12 cycles.

Nyquist plots was equal to the electron transfer resistance (R_{et}) at the electrode interface. The CNTs/GCE exhibited a higher R_{et} than GCE due to the good hydrophobicity (curve a, b). With the sequential assembly of QDs/CH/AuNPs (curve c), Ab_1 (curve d), BSA (curve e), Ag (curve f) and PtAu BNTs−CD@Ada−Ab_2 (curve g), the R_{et} increased steadily. The result of EIS was consistent with that of CV, confirming the successful preparation of the biosensor. The surface topography of modified electrodes surveyed by SEM also demonstrated the successful fabrication of the ECL biosensor (Fig. S2).

3.5. Synergetic amplification of PtAu BNTs and CD-Ada for ECL biosensor

The roles of the three amplifying mediums (CNTs, PtAu BNTs and CD-Ada) were confirmed by comparing the signal intensities of four different biosensors (Fig. 5). The first biosensor with a low ECL intensity can be used as control (curve a). Compared with curve a, the enhanced ECL intensity (curve b) was improved 1.2-fold demonstrating that CNTs could accelerate the electron transfer in the ECL process. After electrostatic adsorption between PtAu BNTs and Ab_2 (curve c), the ECL intensity showed a 2.1-fold enhancement because of the mimic-enzyme catalysis of porous PtAu heterojunction nanotube. The ECL intensity of complete biosensor (curve d) had a 5.1-fold enhancement compared with curve b, which could be attributed to three reasons: (i) the interaction of CD-Ada is greater and more stable than electrostatic adsorption; (ii) CD-Ada act as a "bridge" that could cause outward extension of space from the surface of the antibody, resulting in the reduction of steric hindrance above electrode interface; (iii) more extra Ada decorated on Ab_2 could contact PtAu BNTs-CD, leading to further mimic-enzyme catalysis.

3.6. Characterization of the ECL detection of PRRSV

The ECL behavior of the fabricated biosensor for detection of PRRSV was measured under aforementioned optimized conditions in 0.1 M PB solution with 1 mM H_2O_2. The ECL signal of biosensor was corresponded to PRRSV at different concentrations (Fig. 6A). The ECL signal intensities gradually decreased with decreasing concentrations of PRRSV, indicating that the biosensor are biocompatible and sensitive to target changes.

The standard calibration curve of PRRSV (100X, ~19 μg/mL) detection was illustrated in Fig. 6B. The ECL peak intensities were proportional to the logarithmic value of the PRRSV dilution ratio over a range from$1{:}10^3$ to $1{:}10^6$ (19 ng/mL–19 pg/mL). The linear regression equation was I_{ECL} (au) = 1535.00 × log V_{virus}: V + 9769.64, with the correlation coefficient R^2 = 0.9951.I_{ECL} indicated the ECL peak intensity and V_{virus}: V was the PRRSV dilution ratio. The detection limit (dilution ratio) was roughly calculated to be 5.68×10^{-7} (~10.8 pg/mL) with a signal−to−noise ratio of 3.

3.7. Specificity, reproducibility, stability and recovery of the biosensor

Immune globulin (IgG), albumin bovine (BSA), porcine circovirus type 2 (PCV2) and Enterovirus 71 (EV71) at the same concentration were adopted to test the specificity of the biosensor for PRRSV detection. As shown in Fig. 6C, two stronger ECL signals were obtained from PRRSV sample and mixed sample, while only very weak signals emerged for IgG, BSA, PCV and EV71. Additionally, these two stronger ECL signals were fitted to the linear regression equation. These results demonstrated that the proposed ECL biosensor had a good feasibility and selectivity. Moreover, after incubating immunosensor in PRRSV solution for 1 h, the ECL intensities remained comparatively stable during consecutive cyclic potential scanning, indicating an acceptable stability for ECL detection (Fig. 6D). After storage at 4 °C for 7 days, the biosensor retained 85% of the original ECL response.

3.8. Standard addition recovery experiments of the PRRSV in three negative serums

According to the standard addition method, the recovery test was performed by adding PRRSV to three different serum samples. The ECL signals of three different negative serums as the background interference were deducted before. The results obtained from diluted serum samples before and after adding PRRSV were compared to determine each recovery of PRRSV. The results presented in Table S1 indicated that the recovery ratios of 3 serum samples at different PRRSV content ranged from 101.6 to 109.2%. (analytical precision of RSD ≤ 10%) These results validated the reliability and practicality of this method.

4. Conclusion

In this study, we fabricated a novel near–infrared electrochemiluminesence immunosensor for ultrasensitive detection of PRRSV based on mimic-enzyme catalysis and host-guest recognition. Two conclusions could be drawn for the novel near–infrared electrochemiluminesence immunosensor: (i) the porous PtAu BNTs as a substitute for peroxidase presents a catalytic effect, resulting in great improvement of NIR ECL immunoassay; and (ii) host-guest recognition between β-CD and Ada form a stable "bridge" to link more PtAu BNTs with single antibody, leading to signal amplification. Compared with the traditional veterinary laboratory diagnosis of PRRSV antigen like PCR and indirect immunofluorescent assay, the current method exhibits a higher sensitivity and wider linear range. Therefore, this novel detection method can be used as an alternative tool for clinical diagnosis.

Acknowledgement

We gratefully acknowledge the financial support from National Natural Science Foundation of China (21375043) and National Key Research Development Program of China (2016YFD0500700).

Appendix A. Supplementary data

Supplementary data associated with this article can be found, in the online version, at http://dx.doi.org/10.1016/j.snb.2016.08.162.

References

[1] C.J. Nelsen, M.P. Murtaugh, K.S. Faaberg, Porcine reproductive and respiratory syndrome virus comparison: divergent evolution on two continents, J. Virol. 73 (1999) 270–280.
[2] H. Kim, J. Kwang, I. Yoon, H. Joo, M. Frey, Enhanced replication of porcine reproductive and respiratory syndrome (PRRS) virus in a homogeneous subpopulation of MA-104 cell line, Arch. Virol. 133 (1993) 477–483.
[3] P.F. Gerber, K. O'Neill, O. Owolodun, C. Wang, K. Harmon, J. Zhang, P.G. Halbur, L. Zhou, X.J. Meng, T. Opriessnig, Comparison of commercial real-time reverse transcription-PCR assays for reliable, early, and rapid detection of heterologous strains of porcine reproductive and respiratory syndrome virus in experimentally infected or noninfected boars by use of different sample types, J. Clin. Microbiol. 51 (2013) 547–556.
[4] D.M. Rissin, C.W. Kan, T.G. Campbell, S.C. Howes, D.R. Fournier, L. Song, T. Piech, P.P. Patel, L. Chang, A.J. Rivnak, Single-molecule enzyme-linked immunosorbent assay detects serum proteins at subfemtomolar concentrations, Nat. Biotechnol. 28 (2010) 595–599.
[5] M. Zhang, R. Yuan, Y. Chai, S. Chen, H. Zhong, C. Wang, Y. Cheng, A biosensor for cholesterol based on gold nanoparticles-catalyzed luminol electrogenerated chemiluminescence, Biosens. Bioelectron. 32 (2012) 288–292.
[6] S. Xu, Y. Liu, T. Wang, J. Li, Positive potential operation of a cathodic electrogenerated chemiluminescence immunosensor based on luminol and graphene for cancer biomarker detection, Anal. Chem. 83 (2011) 3817–3823.
[7] K.M. Omer, S.Y. Ku, K.T. Wong, A.J. Bard, Efficient and stable blue electrogenerated chemiluminescence of fluorene-substituted aromatic hydrocarbons, Angew. Chem. Int. Ed. 48 (2009) 9300–9303.
[8] Y. Chi, Y. Dong, G. Chen, Inhibited Ru $(bpy)_3^{2+}$ electrochemiluminescence related to electrochemical oxidation activity of inhibitors, Anal. Chem. 79 (2007) 4521–4528.
[9] G.-X. Liang, L.-L. Li, H.-Y. Liu, J.-R. Zhang, C. Burda, J.-J. Zhu, Fabrication of near-infrared-emitting CdSeTe/ZnS core/shell quantum dots and their electrogenerated chemiluminescence, Chem. Commun. 46 (2010) 2974–2976.
[10] R. Cui, Y.-P. Gu, L. Bao, J.-Y. Zhao, B.-P. Qi, Z.-L. Zhang, Z.-X. Xie, D.-W. Pang, Near-infrared electrogenerated chemiluminescence of ultrasmall Ag_2Se quantum dots for the detection of dopamine, Anal. Chem. 84 (2012) 8932–8935.
[11] J. Wang, H. Han, X. Jiang, L. Huang, L. Chen, N. Li, Quantum dot-based near-infrared electrochemiluminescent immunosensor with gold nanoparticle-graphene nanosheet hybrids and silica nanospheres double-assisted signal amplification, Anal. Chem. 84 (2012) 4893–4899.
[12] G. Zou, H. Ju, Electrogenerated chemiluminescence from a CdSe nanocrystal film and its sensing application in aqueous solution, Anal. Chem. 76 (2004) 6871–6876.
[13] A.J. Stewart, E.J. O'Reilly, R.D. Moriarty, P. Bertoncello, T.E. Keyes, R.J. Forster, L. Dennany, A cholesterol biosensor based on the NIR electrogenerated-chemiluminescence (ECL) of water-soluble CdSeTe/ZnS quantum dots, Electrochim. Acta 157 (2015) 8–14.
[14] K. Shao, J. Wang, X. Jiang, F. Shao, T. Li, S. Ye, L. Chen, H. Han, Stretch–stowage–growth strategy to fabricate tunable triply-amplified electrochemiluminescence immunosensor for ultrasensitive detection of pseudorabies virus antibody, Anal. Chem. 86 (2014) 5749–5757.
[15] W. Gao, H. Dong, J. Lei, H. Ji, H. Ju, Signal amplification of streptavidin–horseradish peroxidase functionalized carbon nanotubes for amperometric detection of attomolar DNA, Chem. Commun. 47 (2011) 5220–5222.
[16] J. Gao, Z. Guo, F. Su, L. Gao, X. Pang, W. Cao, B. Du, Q. Wei, Ultrasensitive electrochemical immunoassay for CEA through host–guest interaction of β-cyclodextrin functionalized graphene and Cu@Ag core–shell nanoparticles with adamantine-modified antibody, Biosens. Bioelectron. 63 (2015) 465–471.
[17] L. Yang, S. Fan, G. Deng, Y. Li, X. Ran, H. Zhao, C.-P. Li, Bridged β-cyclodextrin-functionalized MWCNT with higher supramolecular recognition capability: the simultaneous electrochemical determination of three phenols, Biosens. Bioelectron. 68 (2015) 617–625.
[18] L. Wang, J. Lei, R. Ma, H. Ju, Host–guest interaction of adamantine with a β-cyclodextrin-functionalized AuPd bimetallic nanoprobe for ultrasensitive electrochemical immunoassay of small molecules, Anal. Chem. 85 (2013) 6505–6510.
[19] W.-W. Zhao, Z.-Y. Ma, P.-P. Yu, X.-Y. Dong, J.-J. Xu, H.-Y. Chen, Highly sensitive photoelectrochemical immunoassay with enhanced amplification using horseradish peroxidase induced biocatalytic precipitation on a CdS quantum dots multilayer electrode, Anal. Chem. 84 (2011) 917–923.
[20] Y.-l. Dong, H.-g. Zhang, Z.U. Rahman, L. Su, X.j. Chen, J. Hu, X.-g. Chen, Graphene oxide–Fe_3O_4 magnetic nanocomposites with peroxidase-like activity for colorimetric detection of glucose, Nanoscale 4 (2012) 3969–3976.
[21] Y. Tao, Y. Lin, Z. Huang, J. Ren, X. Qu, Incorporating graphene oxide and gold nanoclusters: a synergistic catalyst with surprisingly high peroxidase-like activity over a broad pH range and its application for cancer cell detection, Adv. Mater. 25 (2013) 2594–2599.
[22] L. Han, C. Li, T. Zhang, Q. Lang, A. Liu, Au@ Ag heterogeneous nanorods as nanozyme interfaces with peroxidase-like activity and their application for one-pot analysis of glucose at nearly neutral pH, ACS Appl. Mater. Inter. 7 (2015) 14463–14470.
[23] J.W. Hong, S.W. Kang, B.-S. Choi, D. Kim, S.B. Lee, S.W. Han, Controlled synthesis of Pd–Pt alloy hollow nanostructures with enhanced catalytic activities for oxygen reduction, ACS Nano 6 (2012) 2410–2419.
[24] B.Y. Xia, H.B. Wu, N. Li, Y. Yan, X.W.D. Lou, X. Wang, One-pot synthesis of Pt-Co alloy nanowire assemblies with tunable composition and enhanced electrocatalytic properties, Angew. Chem. Int. Ed. 127 (2015) 3868–3872.

[25] K. Cai, J. Liu, H. Zhang, Z. Huang, Z. Lu, M.F. Foda, T. Li, H. Han, Facile synthesis of quasi-one-Dimensional Au/PtAu heterojunction nanotubes and their application as catalysts in an oxygen-reduction reaction, Chem. Eur. J. 21 (2015) 7556–7561.
[26] X. Hu, H. Han, L. Hua, Z. Sheng, Electrogenerated chemiluminescence of blue emitting ZnSe quantum dots and its biosensing for hydrogen peroxide, Biosens. Bioelectron. 25 (2010) 1843–1846.

Biographies

Kang Shao was born in Shandong Province, China, in 1987. He is now a PhD in Huazhong Agricultural University under the direction of Professor Heyou Han. His research interests in the synthesis and application of nanostructures for biosensing.

Chenjun Zhang was born in Hubei Province, China, in 1991. She received his MS degree in 2015 in Huazhong Agricultural University under the direction of Professor Heyou Han. Her research interests focus on biosensing and bioimaging.

Shiyi Ye was born in Hubei Province, China, in 1988. She received his BS and Ph.D. degree in 2011 and 2016, respectively in Huazhong Agricultural University under the direction of Professor Heyou Han and Qigai He. Presently she is working as a lecturer at Changjiang University. Her scientific interests focus on biosensing and bioimaging.

Kai Cai was born in Hubei Province, China, in 1986. He received his Ph.D degree in 2016 in Huazhong Agricultural University under the direction of Professor Heyou Han. His scientific interests focus on synthesis and application of nanostructures for biosensing and electrocatalysis.

Wu Long was born in Hubei Province, China, in 1988. He is now a PhD in the School of Food Science and Technology at the Huazhong Agricultural University under the direction of Professor Heyou Han. His scientific interests focus on biosensing.

Biru Wang was born in Hubei Province, China, in 1991. She received his BS degree in Wuhan Institute of Technology in 2015. Her research interests focus on biosensing and bioimaging.

Chenchen Zou was born in Hubei Province, China, in 1990. She received his MS degree in 2016 in Huazhong Agricultural University under the direction of Professor Heyou Han. Her research interests focus on biosensing and bioimaging.

Zhicheng Lu received his Ph.D degree in 2008 in Jilin University. He was a postdoctor in Suzhou Institute of Nano-Tech and Nano-Bionic and Huazhong Agricultural University, consecutively. Presently he is working at Huazhong Agricultural University. His scientific interests focus on synthesis and modification of plasmonic nanostructures for biosensing.

Heyou Han was born in Anhui Province, China, in 1962. He received his Ph.D. degree in Wuhan University in 2000 and he was a postdoctor in Jeckson State University (America) from 2000 to 2004. He has been a Professor of Huazhong Agricultural University since 2004. He has published over 100 papers in international journals. His research interests focus on functionalized nanomaterials for bioanalysis, food safety and energy applications.